
# Dynamics of laser induced metal nanoparticle and pattern formation

R. J. Peláez, T. Kuhn, C. E. Rodríguez, and C. N. Afonso

Citation: Applied Physics Letters **106**, 061914 (2015); doi: 10.1063/1.4908251

View online: http://dx.doi.org/10.1063/1.4908251

View Table of Contents: http://scitation.aip.org/content/aip/journal/apl/106/6?ver=pdfcov

Published by the AIP Publishing



# Dynamics of laser induced metal nanoparticle and pattern formation

R. J. Peláez,[a] T. Kuhn, C. E. Rodríguez, and C. N. Afonso
*Laser Processing Group, Instituto de Óptica, CSIC, Serrano 121, 28006 Madrid, Spain*

(Received 22 December 2014; accepted 4 February 2015; published online 13 February 2015)

Discontinuous metal films are converted into either almost round, isolated, and randomly distributed nanoparticles (NPs) or fringed patterns of alternate non transformed film and NPs by exposure to single pulses (20 ns pulse duration and 193 nm wavelength) of homogeneous or modulated laser beam intensity. The dynamics of NPs and pattern formation is studied by measuring in real time the transmission and reflectivity of the sample upon homogeneous beam exposure and the intensity of the diffraction orders 0 and 1 in transmission configuration upon modulated beam exposure. The results show that laser irradiation induces melting of the metal either completely or at regions around intensity maxima sites for homogeneous and modulated beam exposure, respectively, within $\leq$10 ns. The aggregation and/or coalescence of the initially irregular metal nanostructures is triggered upon melting and continues after solidification (estimated to occur at $\leq$80 ns) for more than 1 $\mu$s. The present results demonstrate that real time transmission rather than reflectivity measurements is a valuable and easy-to-use tool for following the dynamics of NPs and pattern formation. They provide insights on the heat-driven processes occurring both in liquid and solid phases and allow controlling *in-situ* the process through the fluence. They also evidence that there is negligible lateral heat release in discontinuous films upon laser irradiation. © *2015 AIP Publishing LLC*. [http://dx.doi.org/10.1063/1.4908251]

Metal nanoparticles (NPs) either randomly distributed or periodically organised have a high potential for several applications including camouflage, sensors, photovoltaic or optical devices, and tissue engineering scaffolds.[1,2] Most of the applications relate to their unique optical response that is dominated by the surface plasmon resonance (SPR).[3] Heating of metal thin films is a method used since very long to produce them because metal films on dielectric substrates are thermodynamically unstable and tend to dewet for reducing their surface to volume ratio and thus the free energy of the system.[4–6]

Laser techniques offer a faster means not only for producing NPs on a surface by a heat driven process but also for producing periodic structures, thus representing an alternative route to the costly lithographic methods such as electron beam writing,[3] particularly for those applications in which large-scale and low-cost manufacturing is essential. Irradiation with homogeneous or Gaussian converts metal films into nanoislands, beads or NPs and even self-organised structures with well-defined length scales.[7–11] Irradiation with modulated beams such as those produced by beam interference produces structures with controlled motives and periods in large areas ($>$mm$^2$).[12–16] These earlier works aim either to the understanding of the length scales of the dewetting and/or mass flow mechanisms or the fabrication of nanostructures. There is only a very recent work studying the dewetting process in real time upon Gaussian ns laser pulses[11] by using complex pump-probe electron microscopy techniques. As a result, little is known on the dynamics and time scales of the mechanisms governing the NPs or pattern formation upon laser irradiation. In order to fully exploit the capabilities of laser based techniques for producing isolated NPs or periodic structures containing NPs, easy-to-use tools to understand the underlying mechanisms that eventually allow controlling *in-situ* the process are needed. In this letter, we aim to provide direct evidence that the production of NPs and patterns containing NPs by single ns laser pulses are very fast processes both starting upon melting and continuing after solidification in solid-state.

We have used silver samples prepared by pulsed laser deposition in vacuum ($<5 \times 10^{-6}$ mbar) by means of an ArF laser ($\lambda = 193$ nm and $\tau = 20$ ns). The laser beam was focused at 45° on the Ag target leading to a fluence of $\approx$2.7 J cm$^{-2}$ per pulse. The substrates were glass slides held at room temperature, positioned $\approx$38 mm away from the target. They were rotated in order to produce a homogenous deposit over an area $>$1 cm$^2$. The number of laser pulses on the target was selected in order to produce samples with effective metal thicknesses (i.e., the thickness if the silver was forming a continuous layer) of 3.7 nm and 5.9 nm.

The samples were exposed in air to single pulses from the same excimer laser using either a fly's eye lens homogenizing system or a fringed phase mask both manufactured by Laser-Laboratorium Göttingen, which will be referred to from now on as homogeneous and modulated beam exposures, respectively. In the former case, the beam intensity was constant (within 5%) over $\approx 4 \times 4$ mm$^2$ square regions and fluence was varied in the range of 121–309 mJ cm$^{-2}$. In the latter case, a two-lens projection optics was used to expose the sample to an intensity modulated with a period $\Delta = 6.3$ $\mu$m. The average fluence ($\boldsymbol{F} = 78$ mJ cm$^{-2}$) at the sample site is thus modulated along the direction perpendicular to the fringes between 0 and $\boldsymbol{2F} = 156$ mJ cm$^{-2}$. Further details can be found elsewhere.[17]

A He-Ne laser beam pulsed to $\approx$1 $\mu$s by means of an acousto-optic modulator and focused at the irradiated area at

[a]rpelaez@io.cfmac.csic.es

 

≈33° off its normal was synchronized with the irradiation laser pulse in order to record in real time and simultaneously the reflectivity and transmission of the sample upon homogeneous beam exposure. The signals are collected by two fast photodiodes and recorded with a two-channel fast oscilloscope that is triggered by the signal provided by a photodiode collecting a small fraction of the pump beam thus defining the origin of the time scale (it is ≈3 ns earlier than the time at which the pump pulse reaches its maximum at the most). This type of measurements has since very long been applied to record the reflectivity of metals to study melting and solidification processes.[18–20] However, none of these studies report dewetting because they were related to either bulk metals or thick films for which dewetting might not be likely due to the pump laser light absorption length being smaller than the film thickness.

Figure 1 shows transients recorded upon irradiating the 3.7 nm thick sample with 153 mJ $cm^{-2}$. The vertical axis represent the recorded intensity (I(t)) referred to the initial value ($I_i$) as $(I(t) - I_i)/I_i$. It is seen that the transients start with a very rapid decrease and while transmission T(t) soon undergoes a minimum ($T_{min}$), reflectivity R(t) keeps decreasing. After a few tens of ns, R(t) becomes constant within noise and equal to the level recorded after seconds. After $T_{min}$, T(t) instead increases for long time and the whole process is not completed in the time scale, the detection is active (≈1 $\mu$s). The final levels achieved ($R_f$ and $T_f$) are indicated as horizontal traces.

We have looked at the sample structure using a field emission scanning electron microscopy (SEM). The insets in Fig. 1 show that the as grown sample is a discontinuous layer formed by irregularly shaped NPs and coverage of 54% and the metal has converted into almost round NPs of ≈18 nm average diameter with coverage of ≈40% upon irradiation. The extinction spectra were determined as $\ln(1/T(\lambda))$ from transmission spectra ($T(\lambda)$) measured at 0° of incidence

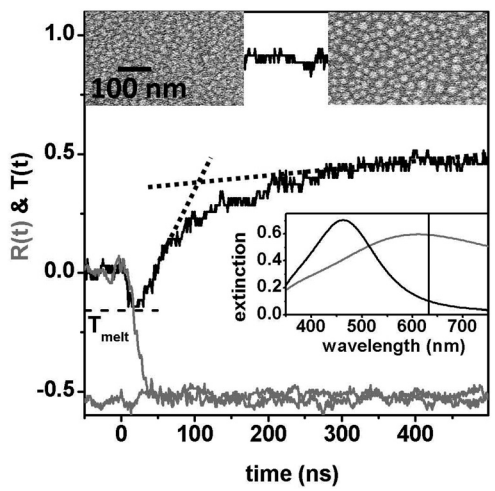


FIG. 1. (Black) T(t) and (grey) R(t) determined upon homogeneous beam exposure the 3.7 nm thick sample with a fluence of 153 mJ $cm^{-2}$; horizontal traces correspond to the final levels achieved and the short horizontal dashed line corresponds to the calculated $T_{melt}$; dotted lines illustrate how the time the change of slope occurs is determined. SEM images of the (left) as grown and (right) laser exposed areas. The extinction spectra of the (grey) as grown sample and (black) the area after laser exposure are shown in the inset where the vertical line corresponds to the laser probe wavelength.

angle with a UV-Vis Cary 5000 dual beam spectrometer. The inset in Fig. 1 shows that while the extinction spectrum of the as grown sample has a very broad SPR band (614 nm). It shifts to the blue (463 nm), becomes more intense, and narrows upon irradiation. The sample becomes almost transparent at the probe beam wavelength thus explaining the high value achieved by $T_f$ in Fig. 1 with respect to $T_i$. The observed changes in the SPR features are also consistent with the changes in the film structure, i.e., the irregularly shaped and almost touching islands of the as grown sample and the almost round and isolated NPs of the sample after irradiation.

The initial decrease of R(t) observed in Fig. 1 is consistent with the widely reported slightly lower reflectivity of liquid metals with respect to solid material.[18–20] We have used the optical constants reported for solid[21] and liquid[22] silver to calculate the expected intensity change upon melting of a 3.7 nm thick layer, the results being $R_{melt} = -0.05$ and $T_{melt} = -0.16$. While the latter agrees very well with $T_{min}$ in Fig. 1, the former is of the order of magnitude of that reported earlier upon melting of metals[18–20] but one order of magnitude smaller than the decrease experimentally observed in Fig. 1 (−0.51). This comparison allows us concluding on the one hand that melting has occurred when T(t) reaches $T_{min}$. On the other hand, the T(t) increase after this point is consistent with the sample becoming eventually more transparent at the probe wavelength (evidenced in the inset of Fig. 1) due to the formation of the NPs. This allows concluding that the agglomeration/coalescence process starts upon melting. Furthermore, T(t) undergoes a change of slope around ≈80 ns after $T_{min}$ to keep increasing at a slower rate afterwards. This behavior is similar to the one reported upon laser cooling of metals and consistent with the onset of solidification.[18–20] However, the fact that the cooling process overlaps in our case with the agglomeration/coalescence of the metal makes it difficult to correlate the T(t) value at the change of slope with the solidification onset in a quantitative way. The stronger decrease of the experimentally measured R(t) with respect to $R_{melt}$ is consistent with this interpretation since reflectivity contains the information of scattering that becomes important once the agglomeration/coalescence process starts. At an intermediate time between $T_{min}$ and the onset of solidification, R(t) becomes blind to the process dynamics since no further changes are observed thus making T(t) much more valuable than R(t) for monitoring the dynamics of NPs formation.

The dynamics dependence on laser fluence was studied in the 5.9 nm thick sample through transmission transients that are shown in Fig. 2(a). Their features are similar to those already discussed in relation to Fig. 1 for the thinnest sample, i.e., a first fast and short decrease down to $T_{min}$ followed by an increase to a $T_f$ level much higher than $T_i$ that is reached in a time longer than ≈1 $\mu$s. $T_f$ values are plot in Fig. 3 as a function of fluence showing they increase sharply in a narrow fluence interval (121–135 mJ $cm^{-2}$), reach a maximum value for 187 mJ $cm^{-2}$ and decrease slightly for higher fluences. The decrease of $T_f$ after the maximum change occurs together with the appearance of a peak within the minimum, making its structure complex as seen in Fig. 2(a). A peak whose width <5 ns is clearly seen for 264 mJ $cm^{-2}$ that

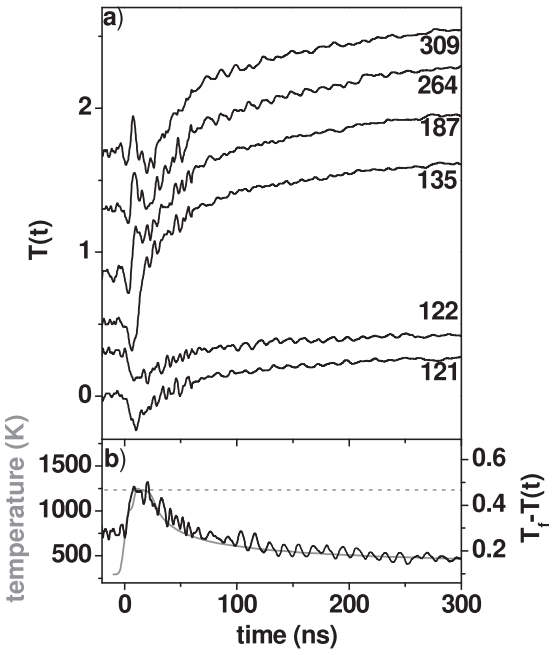


FIG. 2. (a) T(t) determined upon homogeneous beam exposure the 5.9 nm thick sample; the labels indicate the fluence used in mJ $cm^{-2}$; and the transients have been vertically displaced for clarity. (b) (Grey) Calculated temperature-time profile and (black) inverse of T(t) in (a) for 121 mJ $cm^{-2}$; the grey horizontal dashed line is the melting temperature of bulk silver.

starts before $T_{min}$ reaches the value corresponding to the liquid metal. This result together with the fact that this peak is only evident for high fluences suggests that it might be related to the onset of evaporation/ablation.

This reasoning is supported by the laser induced temperature profiles calculated through 3D simulations.[23] The discontinuous character of the samples is taken into account by assuming they are formed by alternate lines of Ag and glass, their width ratio and thickness being determined by the coverage and calculated in order to have mass conservation, respectively. We have assumed the melting (1235 K) and boiling (2435 K) temperatures of bulk silver as well as its latent heat of 11.3 kJ $mol^{-1}$.[24] The thermal conductivity was considered constant and equal to that of the bulk at room temperature. The specific heat was varied from that of the solid to that of the liquid[25] in a temperature interval of ±5 K centred at the melting temperature during which the latent heat was absorbed/released. We have used the optical

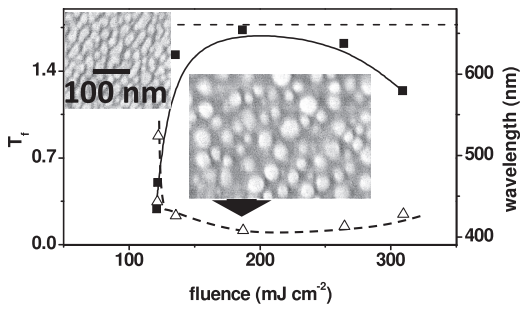


FIG. 3. (■) $T_f$ of the transients in Fig. 2(a) and (△) SPR wavelength as a function of the fluence used to homogeneously expose the 5.9 nm sample; the horizontal dashed line is the SPR wavelength of the as grown sample. The insets are SEM images of the (left) as grown and (center) laser exposed area to 187 mJ $cm^{-2}$ at the same magnification.

constants of bulk solid silver at room temperature[21] and those for the liquid reported in Ref. 22 to calculate the reflectivity and absorption of the Ag lines and used the coverage to simulate the discontinuous character. Figure 2(b) shows the temperature-time profile calculated for the lowest fluence for which a transient could be recorded and thus very close to the threshold fluence. The inverse of the T(t), i.e., $T_f$-T(t), is also included to ease the comparison that shows the calculated temperature time-profile reproduces very well that of the experimental transient. The time at which melting temperature is reached during cooling is smaller than the one deduced from the change of slope of the transient. This result is consistent with the existence of undercooling as reported earlier for Ni films for which calculations suggested an undercooling of 512 K (Ref. 18) although the additional role of a lower melting temperature related to the diameter of the NPs formed upon aggregation/coalescence cannot be ruled completely out.[26] Furthermore, the maximum of the time-temperature profiles reaches the boiling temperature for 264 mJ $cm^{-2}$ supporting that the narrow peak that appears within the minimum in the transients for fluences ≥264 mJ $cm^{-2}$ relates to ablation/evaporation. Although the reason why this process leads to an increase in T(t) is unclear at this stage, it might be related to the formation of a transient plasma whose emission at the probe beam wavelength is not negligible.

The SEM images in the insets of Fig. 3 show that the as grown sample (left) is discontinuous with coverage of 68% that is higher than that of the thinnest sample as expected. After laser exposure to 187 mJ $cm^{-2}$ (right), the metal is forming almost isolated round NPs with an average diameter of 38 nm. The fact that the diameter of the NPs for similar exposure fluences increases as sample thickness increases agrees well with what has earlier been reported in the literature.[9,12,16] Since the extinction spectra before and after laser irradiation are similar to those shown in the inset in Fig. 1 for the thinnest sample, only the evolution of the SPR wavelength with fluence is shown in Fig. 3. It is seen that the SPR shifts to the blue as fluence increases and mirrors the changes in $T_f$.

The times at which $T_{min}$ and the change of slope occur in the T(t) are, respectively, ≤10 ns and ≤80 ns for fluences in the range of 121–187 mJ $cm^{-2}$. The former value agrees very well not only with the calculations but also with the time typically reported for the formation of liquid both in bulk metals[18–20] and metal films having thicknesses comparable to those in the present work.[11] Assuming that the change of slope corresponds to the onset of solidification, both time values lead to a duration of the liquid phase <70 ns that also agrees very well with the values earlier reported for Ni NPs and deduced from time-resolved diffraction patterns collected in a pump-probe electron microscopy experiment.[11] Furthermore, these time scales are also in excellent agreement with the time reported for coalescence of Al aggregates upon laser irradiation.[27] This reasoning supports further our conclusion that agglomeration/coalescence starts upon melting, continues after solidification, and needs more than 1 μs (the cutoff time of the detection system) to complete. The long time duration demonstrates that once agglomeration/coalescence starts, the metal remains heated

for a long time during which the process keeps progressing in solid state at lower rate.

The same set-up has been used to record the intensity of the 0 and 1 diffracted beams in transmission configuration upon modulated beam exposure. The application of this type of measurements to study the dynamics of pattern formation has only very recently applied to patterns produced in porous silicon.[17] Figure 4(a) shows the transients recorded in the 5.9 nm thick sample and while the vertical scale for the signal in order 0 (T0(t)) corresponds to the intensity normalized to the initial, that in order 1 (T1(t)) is the intensity recorded in mV since initial value is cero. The vertical scales have been chosen in order to overlap both final and initial levels, the former been indicated by a single horizontal line. It is also seen that T0(t) is very similar to the T(t) recorded upon homogeneous beam exposure (Fig. 2(a) and the times at which the minimum and the change in slope after the minimum occur are very similar to those determined upon homogeneous beam exposure. This result is consistent with the discontinuous character of the initial sample (Fig. 4(b)) that prevents lateral heat diffusion and thus the temperature profile matches the intensity beam profile.[28] Figures 4(c) and 4(d) show, respectively, optical and SEM images of the pattern produced evidencing that it is formed by alternate fringes having the structure of the as grown material (compare Fig. 4(e) to Fig. 4(b)) and fringes in which the sample has converted into almost isolated round NPs (Fig. 4(f)). The morphology of the latter areas is very similar to what was shown in Fig. 3 upon homogeneous beam exposure for the same sample. The two regions of the pattern will be thus, respectively, referred to as non-transformed and transformed areas.

Since the signal recorded in T1(t) was very weak and comparable to noise, the transient shown in Fig. 4(a) is the average of 7 transients recorded in fresh regions exposed to the same fluence. It becomes clear that T1(t) starts at the same time as T0(t) starts decreasing, i.e., upon melting of the film. This result suggests that a transient pattern due to the alternation of liquid/solid metal as reported earlier for porous silicon[17] has most likely been formed at this very early stage. Once aggregation/coalescence starts (minimum of T0(t)), T1(t) mirrors T0(t), i.e., it increases fast until it undergoes a change of slope at approximately the same time than T0 and needs a time $>1\ \mu$s to reach the final level. This result proves that the long term diffraction is linked to the formation of NPs in the transformed regions and due to the strong shift to the blue and narrowing of the SPR band once isolated NPs are formed upon melting.

In summary, this work shows that the aggregation/coalescence into isolated NPs produced in initially discontinuous metal films by laser irradiation starts immediately upon melting within $\leq$10 ns. The process keeps progressing after the onset of solidification ($\leq$80 ns), lasts for long time ($>1\ \mu$s), and eventually leads to the formation of almost isolated round NPs whose diameter depends on initial sample thickness. Upon modulated beam exposure, a long term pattern formed by alternate fringes of as grown material and NPs is initiated upon melting and continues $>1\ \mu$s. The long-time lasting and similar time scales for the process upon homogeneous and modulated beam exposures are related to the discontinuous character of the samples and the lack of efficient lateral paths for releasing the heat. The sign of the optical changes as a function of time as well as the diffraction efficiency are determined by the plasmonic response of the isolated NPs that shifts blue and narrows with respect to the initial SPR, the higher the fluence the higher the shift. The real time transmission measurements are an easy-to-use tool for *in-situ* controlling the fluence in order to produce tailored NPs or patterns and avoid the ablation regime.

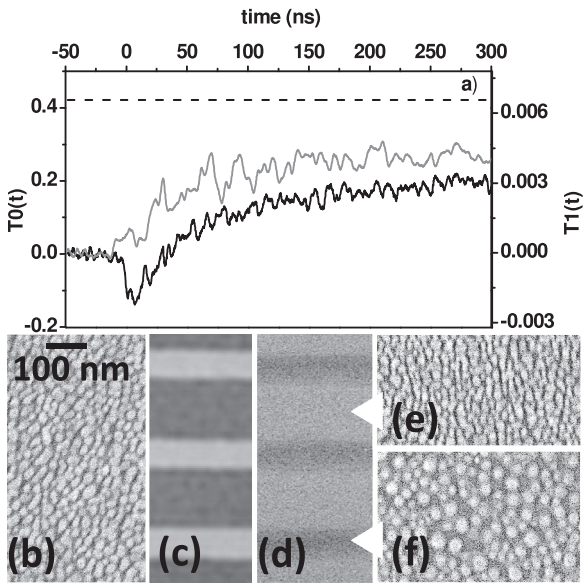


FIG. 4. (a) (Black) T0(t) and (grey) T1(t) determined upon modulated beam exposure in the 5.9 nm sample; the horizontal dashed line corresponds to the final level achieved in both transients. (b) SEM image of the as grown sample. (c) Optical image recorded in transmission and (d) SEM image of the pattern having 6.3 $\mu$m period. SEM images of (e) bright and (f) dark fringes in (d). Images in (b), (e), and (f) have same magnification; idem for (c) and (d).

R.J.P., T.K., and C.E.R., respectively, acknowledge the Grant No. JCI-2012_13034 from the Juan de la Cierva program, the support of DAAD, and CONACYT-México postdoctoral fellowship No. 175641. The authors gratefully thank Professor P. Leiderer from University of Konstanz for his support and the Electron Microscopy Laboratory of CENIM for helping with the SEM observations.

[1]P.-Y. Chen, J. McKittrick, and M. A. Meyers, Prog. Mater. Sci. **57**, 1492 (2012).
[2]H. A. Atwater and A. Polman, Nat. Mater. **9**, 205 (2010).
[3]J. Henzie, J. Lee, M. H. Lee, W. Hasan, and T. W. Odom, Annu. Rev. Phys. Chem. **60**, 147 (2009).
[4]A. E. B. Presland, G. L. Price, and D. L. Trimm, Prog. Surf. Sci. **3**, 63 (1972).
[5]J. Mizsei and V. Lantto, J. Nanopart. Res. **3**, 271 (2001).
[6]D. Gentili, G. Foschi, F. Valle, M. Cavallini, and F. Biscarini, Chem. Soc. Rev. **41**, 4430 (2012).
[7]J. Bischof, D. Scherer, S. Herminghaus, and P. Leiderer, Phys. Rev. Lett. **77**, 1536 (1996).
[8]M. Kawasaki and M. Hori, J. Phys. Chem. B **107**, 6760 (2003).
[9]S. J. Henley, J. D. Carey, and S. R. P. Silva, Phys. Rev. B **72**, 195408 (2005).
[10]C. E. Rodríguez, R. J. Peláez, C. N. Afonso, S. Riedel, P. Leiderer, D. Jimenez-Rey, and A. Climent-Font, Appl. Surf. Sci. **302**, 32 (2014).
[11]J. T. McKeown, N. A. Roberts, J. D. Fowlkes, Y. Wu, T. LaGrange, B. W. Reed, G. H. Campbell, and P. D. Rack, Langmuir **28**, 17168 (2012).
[12]Y. S. Kaganovskii, H. Vladomirsky, and M. Rosenbluh, J. Nanophotonics **1**, 011690 (2007).

[13]S. Riedel, M. Schmotz, P. Leiderer, and J. Boneberg, Appl. Phys. A: Mater. Sci. Process. **101**, 309 (2010).
[14]Z. G. Pang and X. P. Zhang, Nanotechnology **22**, 145303 (2011).
[15]A. K. Gangopadhyay, H. Krishna, C. Favazza, C. Miller, and R. Kalyanaraman, Nanotechnology **18**, 485606 (2007).
[16]R. J. Peláez, C. N. Afonso, J. Bulíř, M. Novotný, J. Lančok, and K. Piksová, Nanotechnology **24**, 095301 (2013).
[17]R. J. Peláez, T. Kuhn, F. Vega, and C. N. Afonso, Appl. Phys. Lett. **105**, 161911 (2014).
[18]H. A. Atwater, J. A. West, P. M. Smith, M. J. Aziz, J. Y. Tsao, P. S. Peercy, and M. O. Thompson, MRS Proc. **157**, 369 (1989).
[19]C. Arnold, M. Aziz, M. Schwarz, and D. Herlach, Phys. Rev. B **59**, 334 (1999).
[20]J. Boneberg, J. Bischof, and P. Leiderer, Opt. Commun. **174**, 145 (2000).
[21]*Handbook of Optical Constants of Solids*, edited by E. D. Palik (Academic, New York, 1985).
[22]S. Krishnan, G. P. Hansen, R. H. Hauge, and J. L. Margrave, High Temp. Sci. **26**, 143 (1990).
[23]COMSOL Multiphysics 4.3 Documentation available at www.comsol.com.
[24]D. R. Lide, *CRC Handbook of Chemistry and Physics*, 82nd ed. (CRC Press LLC, Boca Raton, Florida, 2001).
[25]C. Yang, M. Chen, and Z. Y. Guo, Chin. Sci. Bull. **46**, 1051 (2001).
[26]W. Luo, W. Hu, and S. Xiao, J. Phys. Chem. C **112**, 2359 (2008).
[27]G. C. Egan, K. T. Sullivan, T. LaGrange, B. W. Reed, and M. R. Zachariah, J. Appl. Phys. **115**, 084903 (2014).
[28]R. J. Peláez, C. N. Afonso, M. Škereň, and J. Bulíř, Nanotechnology **26**, 015302 (2015).